Exciton harvesting, charge transfer, and charge-carrier transport in amorphous-silicon nanopillar/polymer hybrid solar cells

Vignesh Gowrishankar,[1,a)] Shawn R. Scully,[1] Albert T. Chan,[1] Michael D. McGehee,[1,b)] Qi Wang,[2] and Howard M. Branz[2]
[1]*Department of Materials Science and Engineering, Stanford University, Stanford, California 94305, USA*
[2]*National Renewable Energy Laboratory (NREL), 1617 Cole Blvd., Golden, Colorado 80401, USA*

(Received 21 August 2007; accepted 15 January 2008; published online 24 March 2008)

We report on the device physics of nanostructured amorphous-silicon (*a*-Si:H)/polymer hybrid solar cells. Using two different polymers, poly(3-hexylthiophene) (P3HT) and poly(2-methoxy-5-(2′-ethyl-hexyloxy)-1,4-phenylenevinylene) (MEH-PPV), we study the exciton diffusion, charge transfer, and charge-carrier transport in bilayer and nanostructured *a*-Si:H/polymer systems. We find that strong energy transfer occurs in the *a*-Si:H/MEH-PPV system. However, inefficient hole transfer from the *a*-Si:H to the polymers renders negligible photocurrent contribution from the *a*-Si:H as well as very small currents in the *a*-Si:H/MEH-PPV devices. These results suggest that *a*-Si:H may be unsuitable for use in polymer-based hybrid cells. Nanosphere lithography and reactive ion etching were used to fabricate nanopillars in *a*-Si:H. The nanostructured *a*-Si:H/P3HT devices showed improved efficiency and almost perfect charge-carrier extraction under short-circuit conditions. By modeling these nanostructured devices, the loss mechanisms were identified and solutions for higher efficiencies are suggested. © *2008 American Institute of Physics*.
[DOI: 10.1063/1.2896583]

INTRODUCTION

The fabrication and performance of amorphous-silicon nanopillar/polymer hybrid composite solar cells, in our work, demonstrates the potential for high efficiency of photovoltaic devices incorporating such ordered nanostructures. The use of polymers in solar cells shows promise for achieving high power-conversion efficiencies at low cost. Polymers have the distinct advantages of being easily solution processable and having high absorption coefficients of greater than 10^5 cm^{-1}. However, they suffer from poor exciton diffusion lengths between 2 and 10 nm, which are significantly smaller than the typical 300–500 nm thicknesses needed by polymers to absorb greater than 90% of the above-bandgap solar photons. Well-studied methods to circumvent this problem include the use of thin tandem solar cells[1,2] and bulk heterojunction solar cells incorporating blends of polymers,[3,4] inorganic nanocrystals and polymers,[5–8] or fullerene (derivatives) and polymers.[9–12] However, such bulk heterojunctions are disordered blends whose internal morphology depends heavily on the physical properties of the polymer and the processing conditions. On the contrary, an ordered inorganic scaffold that is fabricated first, into which a semiconducting polymer is infiltrated, decouples the heterojunction's morphology from the polymer properties and further engenders many distinct advantages. To name a few, an ideal, ordered nanostructure would have (a) a pore radius smaller than the exciton diffusion length to enable maximum exciton harvesting, (b) sufficient thickness (300–500 nm) and minimal volume fraction of the inorganic phase to enable maximum absorption by the polymer, (c) straight pores that provide the most direct paths for charge carriers to their respective electrodes, (d) straight pore walls that likely facilitate polymer chain packing and enhanced hole mobility,[13] and (e) the ability to suitably modify the interface of the inorganic scaffold in order to promote exciton harvesting[14–16] and charge transfer while inhibiting recombination. In the case of hydrogenated amorphous-silicon (*a*-Si:H)/polymer nanostructure systems, charge separation can additionally inhibit recombination within the *a*-Si:H which mitigates the Staebler–Wronksi effect.[17] It is also conceivable that in such a hybrid system, thinner layers of the more expensive inorganic material (than in an all-inorganic device) would be sufficient, thus, reducing the manufacturing cost. In the past, we have attempted to make nanostructured devices by infiltrating poly(3-hexylthiophene) (P3HT) in mesoporous titania[18] but found that the tortuous mesoporous network rendered insufficient polymer hole mobilities for efficient extraction of charges from deep within the mesopores. Ordered nanostructures based on vertically oriented ZnO nanorods[19,20] have also been reported, but large spacing between the nanorods limits the efficiency in these cells.

In this work, we report on the fabrication of *a*-Si:H nanopillars using nanosphere lithography and reactive ion etching that enable smaller pore sizes and straighter pores than those with ZnO nanorods and mesoporous titania, respectively. There are a few compelling reasons to use *a*-Si:H as the inorganic material. Firstly, *a*-Si:H itself has been extensively researched and nanofabrication techniques can be borrowed from the silicon community. Secondly, *a*-Si:H has a strong, complementary absorption spectrum to that of polymers (especially at lower wavelengths) and could, therefore, itself potentially contribute to the photocurrent. Thirdly, it can be easily deposited onto a transparent, conducting sub-

[a)]Electronic mail: vigneshg@gmail.com.
[b)]Electronic mail: mmcgehee@stanford.edu.

strate, thus, obviating the need to deposit a transparent conductor, such as Al-doped ZnO, on top. In terms of device performance of the *a*-Si:H/polymer systems, we first find, unexpectedly, that *a*-Si:H contributes only negligibly to the photocurrent because of inefficient hole transfer to the polymer. Exciton harvesting from the polymer can occur via two mechanisms—exciton diffusion followed by electron transfer and energy transfer from the polymer to the *a*-Si:H. In the case of *a*-Si:H/poly 2-methoxy-5-(2′-ethyl-hexyloxy)-1,4-phenylenevinylene (MEH-PPV), we find significant energy transfer but surprisingly low currents. To explain these results, we deduce that the hole transfer from *a*-Si:H to the polymers is very poor, despite apparently suitable energy levels. The nanostructured *a*-Si:H/P3HT devices show a twofold improvement in the short-circuit current (compared to bilayer devices), while exhibiting almost perfect carrier extraction with no apparent losses from bimolecular recombination or space charge. Based on these findings and their in-depth analyses, we make recommendations for improvements in ordered nanostructure polymer composite solar cells.

EXPERIMENTAL DETAILS

Intrinsic *a*-Si:H was deposited using a hot-wire chemical vapor deposition technique,[21] in which a W filament is heated to about 2000 °C and silane precursor gas is decomposed onto a substrate at ~200 °C. 20 nm of *a*-Si:H was deposited on flat indium-tin-oxide coated glass (bottom electrode) for making bilayer devices.[22] 3 nm of *a*-Si:H on plain glass was used for photoluminescence (PL) quenching studies. For the nanostructured *a*-Si:H/polymer devices, the initial thickness of the *a*-Si:H layer was 100 nm. The 100-nm-thick titania layers used in the bilayer devices were deposited on fluorine-doped tin-oxide-coated glass (bottom electrode) using a sol-gel method reported previously.[23]

Nanostructuring of the *a*-Si:H was performed using nanosphere lithography and reactive ion etching. Polystyrene nanospheres (diameter of $\sim 26 \pm 5.5$ nm) were purchased from Interfacial Dynamics Corp. By adjusting the dilution of the original nanosphere suspension and the speed of the spin coating (typically, approximately two times dilution and 5000 rpm, respectively), a monolayer of the spheres was obtained on the *a*-Si:H surface, which was confirmed using scanning electron microscopy (SEM). 5 nm of Cr was evaporated on this nanosphere monolayer using electron-beam evaporation. The spheres were then dissolved away by sonication for 1–2 h in heated toluene; such a vigorous lift-off technique was required because the Cr coating atop the small nanospheres left very little polystyrene exposed to the solvent. After liftoff, the *a*-Si:H had isolated islands of Cr, which had penetrated the nanosphere monolayer through the interstices between the spheres. The *a*-Si:H was then reactive-ion-etched (RIE) as reported previously.[24] Briefly, NF_3, which selectively attacks Si, was used at low chamber pressure and high bias voltage to achieve anisotropic nanopillars and nanoridges with straight sidewalls. The nanopillar surface was cleaned using UV-ozone treatment to remove

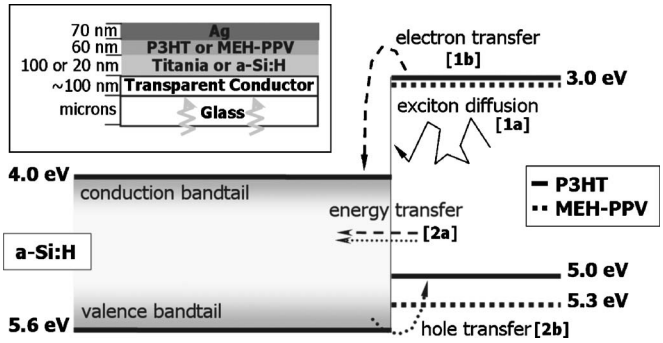

FIG. 1. Vacuum-referenced energy levels of MEH-PPV (Ref. 28), P3HT (Ref. 14), and *a*-Si:H (Ref. 29). Titania (levels not shown) has conduction and valence band edges at ~4.2 and ~7.4 eV, respectively. Energy levels of *a*-Si:H are approximated from the mobility edges, but exponential tails of localized states (bandtails, in graded gray) extend into the mobility gap (Ref. 29). Two mechanisms for exciton harvesting are shown, (1a) exciton diffusion followed by (1b) electron transfer and (2a) energy transfer (this cannot occur in titania/polymer cells) followed by (2b) hole transfer. (Inset) Schematic diagram of the bilayer devices studied.

residue from the etching step.[24] Any remaining Cr was removed by using a standard Piranha etch (80% concentrated sulfuric acid and 20% hydrogen peroxide, by volume), which also oxidized the *a*-Si:H surface. This layer of oxide was removed by dilute hydrofluoric acid treatment, leaving bare *a*-Si:H exposed for subsequent coating by the polymer. A similar hydrofluoric acid treatment was also done for all 20-nm-thick *a*-Si:H substrates used in bilayer devices and certain *a*-Si:H substrates used for the PL quenching studies.

P3HT and MEH-PPV were used in the various experiments. P3HT (approximately 50 000 g/mol molecular weight) was purchased from Rieke Metals and purified by Soxhlet extraction before use. MEH-PPV (approximately 50 000 g/mol molecular weight) was purchased from American Dye Source (Catalog No. ADS100RE) and used as received. 60-nm-thick layers of both polymers were used in the bilayer devices,[22] while different sub-25-nm thicknesses were used for PL quenching experiments. These films were spin coated from solutions in tetrahydrofuran of different concentrations. Only P3HT was used to fabricate devices with the nanostructured *a*-Si:H. About 100 nm of P3HT was spin coated on top of the nanostructured *a*-Si:H. Subsequent infiltration of the P3HT into the nanostructure was performed by heating at 185 °C for 8 min (the glass-transition temperature of P3HT is approximately 25 °C)[25] and slow cooling, both in an inert atmosphere. To complete device fabrication, 70 nm of Ag was evaporated onto the polymer layer to form the top electrode. Schematics of the bilayer and nanostructured devices are shown in Fig. 1 (top left) and Fig. 5(c), respectively. The completed devices were annealed at 135 °C for 3–10 h in an inert atmosphere to obtain optimal photovoltaic performance, as determined with a Spectra-Physics 81150 solar simulator operated at AM 1.5 G conditions with spectral mismatch accounted for. The light intensity was varied by using a series of neutral density filters with flat wavelength responses.

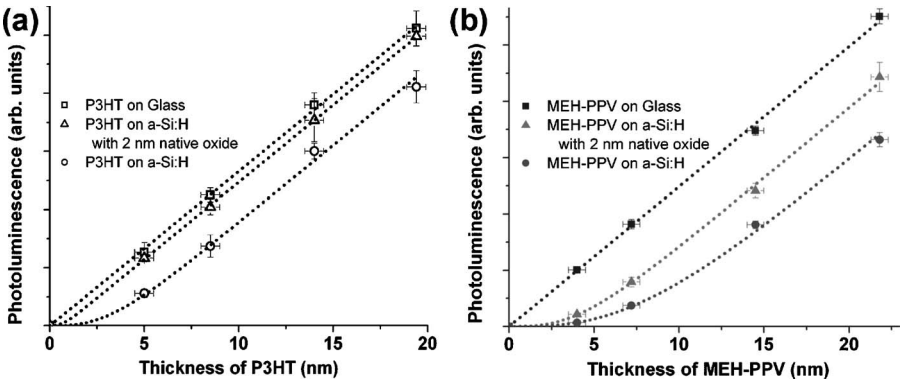

FIG. 2. (a) Photoluminescence data of P3HT as a function of the film thickness. PL data of P3HT on three different substrates, viz., glass (open squares), *a*-Si:H with 2 nm native oxide (open triangles), and bare *a*-Si:H (open circles). (b) Similar photoluminescence data for MEH-PPV films on the three substrates (corresponding filled symbols).

RESULTS AND DISCUSSION

Exciton harvesting and charge transfer in *a*-Si:H/polymer solar cells

We first explore the exciton harvesting processes that can occur within these inorganic/organic hybrid solar cells. Titania is nonabsorbing over wavelengths in the visible spectrum. Following absorption in the semiconducting polymer, bound electron-hole pairs (excitons) are created. Absorption by the *a*-Si:H, however, creates electron-hole pairs that are likely unbound due to exciton binding energies under 0.1 eV.[26] Nevertheless, for reasons explained in detail later, only a very small fraction of photons absorbed in the *a*-Si:H actually contribute to the photocurrent. Therefore, the excitons generated within the polymer mainly contribute to the photocurrent in all the hybrid cells explored. These excitons can be harvested by two mechanisms that are schematically depicted in Fig. 1. In the first mechanism, exciton diffusion to the polymer-inorganic interface is followed by forward electron transfer from the polymer to the inorganic semiconductor. This mechanism is enhanced by large exciton diffusion lengths and a suitable offset between the polymer lowest unoccupied molecular orbital and the inorganic conduction band edge. In the second mechanism, Förster[27]-like energy transfer occurs, wherein excitons in the donor semiconductor (polymer) are transferred to the acceptor semiconductor (inorganic),[14] followed by hole transfer from the inorganic back to the polymer. In both mechanisms, the final state is an electron in the inorganic semiconductor and a hole in the polymer, and these carriers are collected at the electrodes. For energy transfer, the donor energy gap must be larger than the acceptor bandgap, implying that the energy transfer is possible from MEH-PPV and P3HT (energy gaps of ~2.3 and ~2.0 eV, respectively)[14,28] to *a*-Si:H (bandgap of ~1.6 eV),[29] but not to titania (bandgap of ~3.2 eV).

Strong energy transfer from MEH-PPV to *a*-Si:H

Förster[27]-like energy transfer can be envisaged as the radiationless transfer of energy from an excited donor dipole (e.g., exciton in the polymer) to an acceptor dipole (e.g., those in *a*-Si:H). Energy transfer to inorganic semiconductors has been theoretically treated[30] and experimentally observed from organic materials[31] previously. We explored the possibility of energy transfer from the polymers to the *a*-Si:H using a modified framework based on Förster resonant-energy-transfer theory. The rate of energy transfer from a donor dipole to a slab of acceptor dipoles scales as $k_{\text{energy transfer}}\alpha(R_0^6/r^3)$.[15] r is the perpendicular distance between the donor dipole and the slab of acceptor dipoles. R_0 is a characteristic distance that is described by $R_0=[(9000\ln(10)\kappa^2 Q_D/128\pi^5 n^4 N_A)\int_0^\infty \varepsilon_A(\lambda)F_D(\lambda)\lambda^4 d\lambda]^{1/6}$. It depends on the donor fluorescence quantum efficiency (Q_D), the dipole orientation factor (κ^2), the refractive index of the donor-acceptor medium (n), wavelength of light (λ), donor emission spectrum [$F_D(\lambda)$], and the acceptor molar absorptivity [$\varepsilon_A(\lambda)$]. If we assume that the values of κ^2 and n are roughly equivalent for the two *a*-Si:H/polymer systems, we find that the difference in R_0 values for the two systems depends mainly on the Q_D of the polymers. Depending on the batch of MEH-PPV used, it has a reported Q_D between 0.10 and 0.15, while P3HT has a much lower reported Q_D of 0.02.[4] Using approximate estimates of the upper and lower bounds for n (4 and 2 respectively), the calculated ranges of R_0 were between 1.5 and 2.5 nm for *a*-Si:H/MEH-PPV and between 0.9 and 1.7 nm for *a*-Si:H/P3HT. MEH-PPV was, thus, expected to exhibit stronger energy transfer to the *a*-Si:H than P3HT due to the sixth power of R_0 appearing in the energy transfer rate equation, above. To confirm this, we conducted photoluminescence quenching experiments of thin (~25 nm or less) polymer films on glass, *a*-Si:H, and *a*-Si:H with native oxide (henceforth referred to as *a*-Si:H oxide). In order to minimize complications from optical interference effects,[32] the *a*-Si:H layer, which has a large refractive index and is highly absorptive, was kept very thin (~3 nm). Figure 2 shows that the PLs of both polymers on glass are linearly dependent on film thickness, which is as expected for thin films on a nonquenching substrate such as glass. This result implies that neither electron transfer nor energy transfer occurs between the polymers and glass. In the case of P3HT, negligible PL quenching is observed on the *a*-Si:H-oxide substrates, indicating that neither electron transfer nor energy transfer is significant. In the case of MEH-PPV, however, significant PL quenching is observed on the *a*-Si:H-oxide substrates. We assume, realistically, that the native oxide layer is a poor electron acceptor and negligible electron tunneling through the oxide layer occurs. The first assumption is justified by two observations: (1) the PL of the polymer films on chemically similar glass (SiO_2) is not quenched by electron transfer and (2) the PL of P3HT is only slightly quenched (*vide infra*: adequately accounted for by energy transfer directly to the *a*-Si:H and not suggesting electron transfer to the oxide layer) and not significantly

quenched like with MEH-PPV. Therefore, the only reasonable explanation for the substantial PL quenching of MEH-PPV on *a*-Si:H-oxide is the occurrence of energy transfer from MEH-PPV to *a*-Si:H Using the equation for the energy transfer rate ($k_{\text{energy transfer}}$), in conjunction with the natural decay rate, we can calculate the probability of energy transfer for different donor dipole–*a*-Si:H separation distances (r) and then integrate over these distances for the cumulative probability of energy transfer for a given polymer film thickness.[15] By fitting these calculations to the observed PL quenching data, we extract a R_0 of 1.9 nm for the *a*-Si:H/MEH-PPV system, which agrees well with the theoretically predicted values. A similar analysis for *a*-Si:H/P3HT yields a R_0 of ~1 nm for this system. For both polymers, greater PL quenching is observed on bare *a*-Si:H because exciton diffusion followed by electron transfer additionally contributes to the quenching. The fraction of excitons that are quenched by energy transfer versus electron transfer can be modeled by solving the continuity equation as we have reported previously,[15] together with our experimentally determined values of R_0. We use diffusion lengths of 6 and 3 nm for MEH-PPV (Ref. 32) and P3HT,[16] respectively. The occurrence of energy transfer, in addition to electron transfer after exciton diffusion to the interface, would allow for a greater number of excitons to be quenched (harvested) than if only exciton diffusion and electron transfer occurred. Keeping this in mind, in the case of MEH-PPV, we find that at least 80% of quenched excitons undergo energy transfer, while the total number of excitons quenched by both mechanisms together is about 15% greater than if only exciton diffusion and electron transfer were active. In the case of P3HT, the results are less definitive, but at least 30% of quenched excitons are quenched by energy transfer, while the total number of excitons quenched by both mechanisms together is about 30% larger than if only exciton diffusion and electron transfer were active. For more accurate computation of transfer fractions by energy transfer and electron transfer, a quantum-mechanical approach is required, which is beyond the scope of this work. We, thus, find that MEH-PPV undergoes energy transfer to *a*-Si:H much more strongly than P3HT, and most quenched excitons in *a*-Si:H/MEH-PPV are quenched by energy transfer.

Key bilayer (planar) results explained by mechanisms involving energy transfer

In order to understand electron and hole transfer between the polymers and *a*-Si:H, bilayer (planar) devices with thicker, 20 nm *a*-Si:H layers were fabricated. As references, titania/polymer bilayer devices were also fabricated. Since *a*-Si:H and titania have higher electron affinities than the polymers, electron transfer occurs from the polymers to the inorganics. However, hole transfer must occur from *a*-Si:H to the polymer for electron-hole pairs generated within the *a*-Si:H to contribute to the photocurrent. Figure 3 shows the photocurrent-action spectra of the *a*-Si:H/polymer systems along with the relevant absorption spectra. The photoresponse of the titania/polymer cells (not shown) is entirely due to absorption within the polymer.[22] In the case of

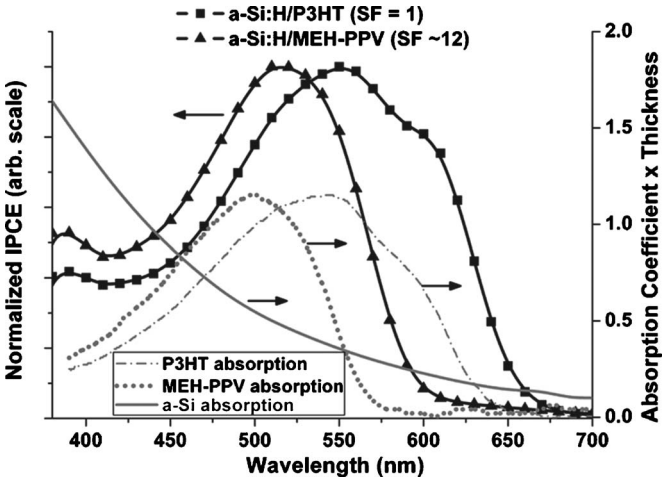

FIG. 3. Normalized photocurrent-action spectra [incident photon to converted electron efficiency (IPCE)] of *a*-Si:H/MEH-PPV (filled triangles) and *a*-Si:H/P3HT (filled squares). Also shown, in the lower part of the graph, are the absorption spectra (absorption coefficient x thickness) of MEH-PPV (dotted gray line), P3HT (dashed gray line), and *a*-Si:H (solid gray line). The polymer films are 60-nm-thick, whereas the *a*-Si:H is 20-nm-thick. SF denotes the scaling factors used to normalize the photocurrent-action spectra: the MEH-PPV spectrum is multiplied by a factor of ~12. Therefore, to make a relative comparison between the *a*-Si:H/P3HT and *a*-Si:H/MEH-PPV photocurrent-action spectra, the latter needs to be divided by a factor of ~12.

a-Si:H/polymer cells, a low-wavelength (<450 nm) shoulder is observed in the photoresponse curves, suggestive of photocurrent contribution from the *a*-Si:H. However, for *a*-Si:H/P3HT, it was deduced that less than 2%–3% of photons absorbed by the *a*-Si:H, over the range of wavelengths shown, actually contributed to the photocurrent. This inference was arrived at by a detailed deconvolution of the photocurrent contributions from the constituent semiconductors. In other words, the photocurrent contributions from the *a*-Si:H and P3HT were calculated based on the overlap between their respective absorption spectra and the solar spectrum. The calculated contribution closely matched with experimental data when the diffusion length of P3HT was 3 nm (Ref. 16) and when only 2%–3% of excitons generated within *a*-Si:H were extracted. This implies that the hole transfer is very poor from *a*-Si:H to P3HT. Even worse hole transfer in the *a*-Si:H/MEH-PPV system renders the photocurrent from the *a*-Si:H even lower, by a factor of 8. The reason for this, as we will show in detail later, is due to the small valence band—highest occupied molecular orbital (HOMO) energy offset between *a*-Si:H and MEH-PPV. Table I shows the salient device characteristics of the *a*-Si:H/polymer and titania/polymer devices. The very low short-circuit current (J_{SC}) and efficiency of the *a*-Si:H/MEH-PPV system were initially surprising to us. Such a low J_{SC} could not be adequately explained by considering only a mechanism of exciton diffusion followed by electron transfer, even after accounting for optical interference effects and possible complications from space charge.[22]

We propose a model that adequately explains these various results. Relevant to the discussion, a schematic energy diagram showing the various transfer processes is shown in Fig. 4. It is well-known that *a*-Si:H has an exponential band-

TABLE I. Short-circuit current (J_{SC}), open-circuit voltage (V_{OC}), fill factor, and power-conversion efficiency of the four bilayer hybrid inorganic-organic systems studied, at a light intensity of 1 sun.

Inorganic	Polymer (60 nm)	J_{SC} (mA/cm^2)	V_{OC} (mV)	Fill factor	Efficiency (%)
a-Si:H	P3HT	−0.64	555	0.57	0.20
Titania	P3HT	−0.72	585	0.62	0.26
a-Si:H	MEH-PPV	−0.04	615	0.26	0.01
Titania	MEH-PPV	−0.37	685	0.31	0.08

tail of localized states extending into the bandgap from the valence band edge due primarily to Si–Si bond-angle disorder. This bandtail will trap a high density of injected or photoexcited holes in localized electronic states. Under our 1 sun illumination conditions, there is significant hole occupation only above the hole-quasi-Fermi level, which is about 0.5 eV above the intrinsic *a*-Si:H valence band edge.[33] To cross from *a*-Si:H to the polymer, these holes deep in the valence bandtail must jump to the polymer HOMO. The number of bandtail holes for which a jump to the HOMO is energetically favorable depends on the HOMO level and the hole-quasi-Fermi level. The reported vacuum-referenced HOMO values for MEH-PPV and P3HT are ~5.3 eV (Ref. 28) and ~5.0 eV,[14] respectively. It is, thus, expected that the hole transfer from *a*-Si:H to MEH-PPV is significantly poorer than that to P3HT, as we observed. Alhough hole transfer to P3HT is so slow that no more than 2%–3% of the photogenerated holes make it across the interface and subsequently to the electrode, hole transfer to MEH-PPV is even worse. Reasons for the weak hole transfer to P3HT include very low (<0.1 eV at most) drop in energy for the holes to cross the interface and, perhaps more crucially, the physical localization of most holes away from the interface due to the low density of valence bandtail states occupied at 1 sun in *a*-Si:H. The even smaller photocurrent contribution from

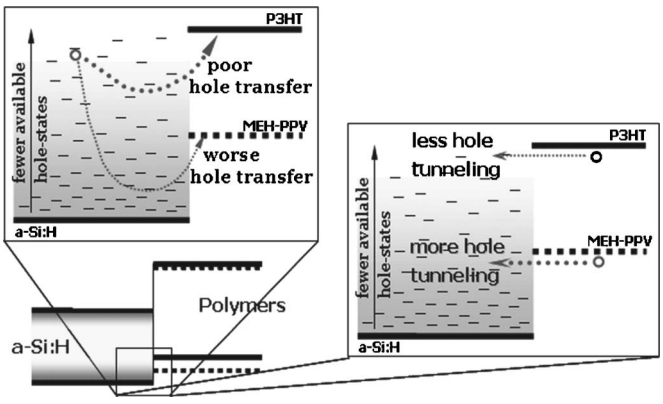

FIG. 4. Mechanisms of hole transfer between *a*-Si:H and the polymers. The short dashes in the *a*-Si:H valence bandtail represent localized hole states. (Top left) Poor hole transfer from *a*-Si:H to P3HT due to low energy drop coupled with probable physical localization of the hole away from the *a*-Si:H/polymer interface. Even worse hole transfer from *a*-Si:H to MEH-PPV (than to P3HT) due to more unfavorable energetics as a result of the higher ionization potential of MEH-PPV (than of P3HT). (Right) The mechanism of deleterious hole tunneling from polymers to *a*-Si:H which can lead to recombination with electrons in the *a*-Si:H. Hole tunneling is greater from MEH-PPV to *a*-Si:H (than from P3HT) because of the larger density of available hole states in the *a*-Si:H for holes to tunnel into from the MEH-PPV HOMO level (than from the P3HT HOMO level).

a-Si:H in *a*-Si:H/MEH-PPV is due to a likely need for holes at the *a*-Si:H quasi-Fermi level to move up in energy to transfer to the MEH-PPV. The poor hole transfer explains why *a*-Si:H/MEH-PPV has such a low J_{SC} despite the high probability of energy transfer from MEH-PPV to *a*-Si:H Any excitons undergoing energy transfer to the *a*-Si:H are essentially "lost" from photoconduction. The consideration of strong energy transfer followed by inefficient hole transfer in the *a*-Si:H/MEH-PPV systems accounts almost entirely for the low J_{SC}. We believe that there is a second loss mechanism—tunneling of holes from MEH-PPV to *a*-Si:H valence bandtail states, followed by recombination with the electrons in the *a*-Si:H. With the HOMO levels and *a*-Si:H bandtail hole occupation as described above, we expect holes to tunnel into electron-occupied *a*-Si:H valence bandtail states from MEH-PPV. The tunneling rate will be increased by Coulomb attraction from any trapped electrons near the *a*-Si:H interface after their transfer from the MEH-PPV. However, the contribution of this hole-tunneling mechanism toward the lost excitons is likely small, given the high likelihood of energy transfer from MEH-PPV to *a*-Si:H (as evidenced by substantial PL quenching of the MEH-PPV on *a*-Si:H-oxide, described earlier).

Nanostructured *a*-Si:H/P3HT solar cells show increased efficiency

Nanostructured *a*-Si:H/P3HT solar cells were fabricated as described earlier. The SEM of the *a*-Si:H nanostructure in Fig. 5(a) shows that the pores are approximately 30–40 nm wide. Figures 5(b) and 5(c) shows a cross-sectional SEM image and a schematic of the nanostructured *a*-Si:H/P3HT device, respectively. The current-voltage (*I-V*) curves of the nanostructured devices along with relevant reference device are shown in Fig. 6(a). A planar reference device with 20 nm of *a*-Si:H generates a J_{SC} of approximately 0.6 mA/cm^2. The other four *I-V* curves are of those devices that have undergone nanosphere lithography and RIE steps. Increasing durations of RIE yielded larger nanostructure heights. The device that underwent a very short duration of RIE (~15 s) had a J_{SC} of ~0.3 mA/cm^2, whereas the device that underwent a RIE of 3 min showed the highest J_{SC} of 1.23 mA/cm^2. The nanostructure heights labelling the *I-V* curves of Fig. 6(a) were measured from SEM images of unfinished devices that had undergone the same durations of RIE. Starting with a 100-nm-thick *a*-Si:H layer, we were unable to etch for longer than about 3 min (corresponding to nanostructure height of 80 nm), before encountering shorting problems in our devices, likely due to penetration of pinholes

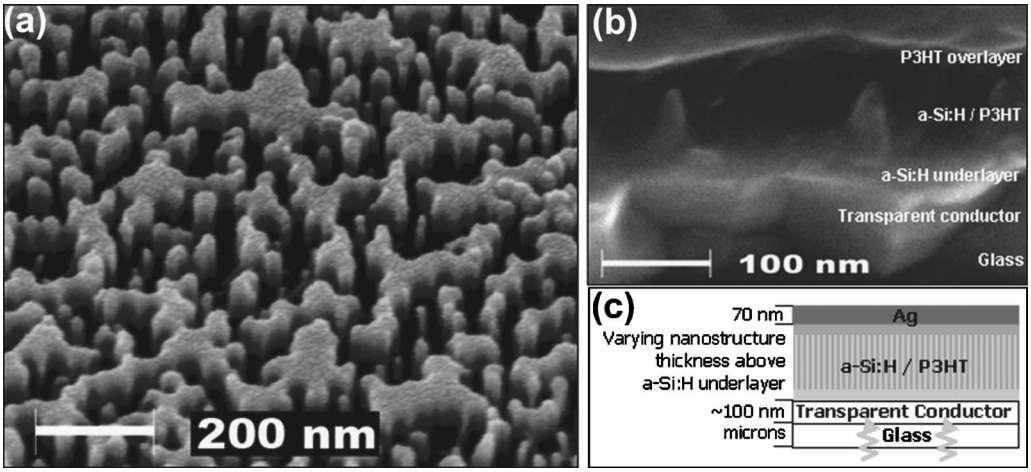

FIG. 5. (a) SEM image of nanostructures in *a*-Si:H taken at a 45° angle. The structure can be best described as an interconnected array of nanoridges and nanopillars, with nominal "pore" sizes (lateral) of 30–40 nm. (b) A cross-sectional SEM image of the *a*-Si:H/P3HT nanostructure after melt infiltration of the P3HT. Pointed nanopillars of *a*-Si:H are clearly seen with P3HT in between. (c) Schematic of the nanostructured *a*-Si:H/P3HT devices studied.

completely through the *a*-Si:H. The best device was, thus, the one with a nominal 20-nm-thick *a*-Si:H planar underlayer beneath an 80-nm-thick nanostructured layer. This device produces twice the photocurrent of the bilayer reference device (also with a 20 nm planar *a*-Si:H layer), attributable directly to the increased interface area between the *a*-Si:H and P3HT. The efficiency of this best nanostructured device was 0.3%. The planar reference device that had not undergone any lithography or RIE steps had a V_{OC} about 90 mV larger than those of the other four devices that had undergone these steps. This difference is likely due to a change in the *a*-Si:H surface chemistry caused by the gases during RIE or by the chemicals used for Cr removal. Among the RIE-etched devices, however, the V_{OC} is seen to increase a few millivolts with nanostructuring, likely due to increasingly thinner underlayers that allow higher intensities of light through to the infiltrated P3HT.

A 25% higher photocurrent is seen at reverse bias (saturated photocurrent at −1.5 V, not shown) than that under short-circuit conditions (0 V). Such higher currents at reverse bias are seen not only for the best nanostructured device but also for all the other nanostructured devices shown in Fig. 6(a). There are four mechanisms that can, in principle, account for reverse-voltage-dependent collection in these cells: (1) improved charge separation of bound, "geminate" pairs[34,35] at the interface after charge transfer, (2) field-assisted dissociation of excitons away from the interface;[1] (3) space charge limitation of current, and (4) bimolecular recombination between free electrons and holes. We believe that the separation of the geminate pairs is a voltage-dependent step in our devices, which is enhanced by higher fields, under reverse-bias conditions. Although different thicknesses of the semiconductor layers in the various devices could lead to differences in the field experienced by the geminate pairs at the *a*-Si:H/P3HT interface, we disregard any little significance this effect might have. We justify our stance by pointing out that the polymer thicknesses in the various devices do not vary greatly. Consequently, by implicitly assuming that most of the voltage drop occurs in the polymer regions, we believe that the field experienced by the

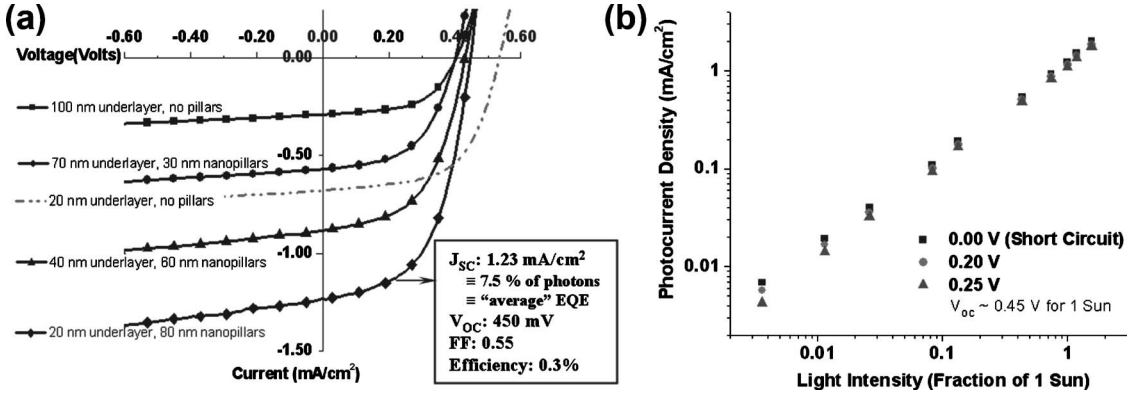

FIG. 6. (a) Current-voltage (*I-V*) curves of the nanostructured *a*-Si:H/P3HT devices (filled symbols) and the reference bilayer device (broken line). Starting with 100 nm of *a*-Si:H, with increasing RIE times, taller nanopillars are obtained while thinner underlayers remain. Progressively larger currents are seen in devices with taller nanopillars, as shown for nanopillar heights of 0 nm (squares), 30 nm (circles), 60 nm (triangles), and 80 nm (diamonds). (b) Log-log plot of photocurrent density vs light intensity for the best nanostructured device (80-nm pillars) at three different bias voltages. The linear relationship between the photocurrent and light intensity suggests bimolecular recombination and space charge problems are negligible over this voltage range. This is confirmed by performing linear fits of the data (not shown) which reveal that the slopes, at all three voltages, are almost perfectly unity within experimental error (between 0.99 and 1.01).

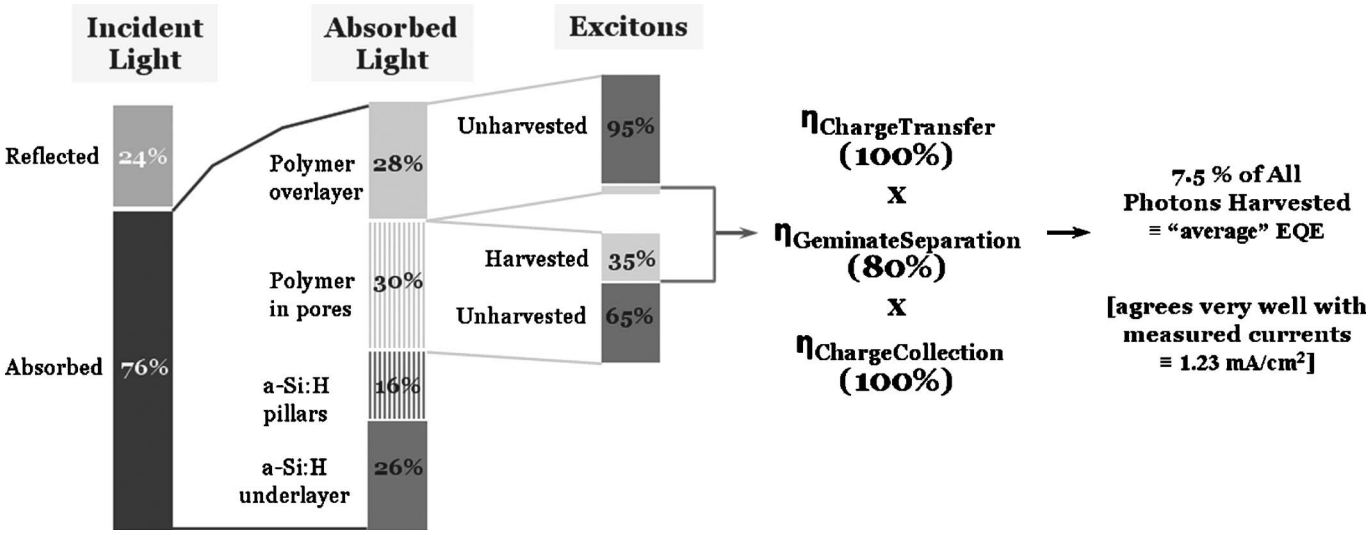

FIG. 7. Quantitative breakdown of efficiencies of the various stages of charge collection under short-circuit conditions, for the best nanostructured device. The optical analysis is done over a range of wavelengths from 400 to 675 nm. The numbers represent the percentages of photons or excitons in various regions or the efficiencies of the various steps, based on our experiments and modeling (independent of J_{SC} measurements).

geminate pairs is similar in all the devices. Exciton dissociation away from the interface (mechanism 2, above) is largely negligible, especially at low field strengths on the order of 10^5 V/cm,[1] typical in such devices under short-circuit conditions. To evaluate the third and fourth alternative hypotheses of space charge limitation and bimolecular recombination causing reverse-voltage-dependent collection within the best nanostructured *a*-Si:H/P3HT device, the photocurrent (current under illumination minus current in the dark) density as a function of light intensity was measured, as shown in Fig. 6(b). The photocurrent was found to be almost perfectly linear with light intensity, even over nearly 3 decades of variation of the illumination intensity (0.003–1.5 suns). This finding suggests that both bimolecular recombination and the photocurrent-limiting effects of space charge are negligible[36–38] because both these phenomena would result in a sublinear dependence of the photocurrent on light intensity, albeit to different extents. We, therefore, conclude from the increased photocurrent at reverse bias and linear dependence of photocurrent with light intensity that, under short-circuit conditions, charge extraction within the best nanostructured device is almost perfectly efficient, while geminate separation is only approximately 80% efficient.

Identification of the loss mechanisms and possible solutions

We have shown that the nanostructuring raises the efficiency of *a*-Si:H/P3HT devices. Nonetheless, the efficiencies are disappointingly low. A detailed analysis of the various steps and their efficiencies, from illumination to charge extraction at the electrodes, elucidates the loss mechanisms in these cells and suggests possible solutions. The sequence of steps that leads to extracted photocurrent is light absorption followed by exciton harvesting (exciton diffusion to an interface followed by electron transfer and/or energy transfer followed by hole back transfer), geminate separation, and finally, charge extraction at the electrodes. For the best nanostructured *a*-Si:H/P3HT device, we display schematically in Fig. 7 the result of the quantitative modeling of the efficiency of each of the steps, based on our optical and electrical measurements (independent of J_{SC} measurements). Since our model accounts for all incident photons in the 400–675 nm wavelength range, the final percentage of incident photons that are converted to electrons represents an "average" external-quantum-efficiency. The percentage of reflected and absorbed light (in different regions) was calculated based on a detailed optical model,[32] while the percentage of excitons harvested was based on simple geometric calculations, and the efficiencies of the other steps were based on inferences presented earlier in this work. Figure 7 shows that 76% of incident photons are absorbed, 40% of which are absorbed by *a*-Si:H, and the rest by P3HT within and on top of the pores. About 35% of excitons generated in the polymer within the pores and 5% of excitons generated in the polymer overlayer diffuse to the *a*-Si:H/P3HT interface. We assume that all these excitons undergo charge transfer across the interface (exciton diffusion followed by electron transfer dominates energy transfer in *a*-Si:H/P3HT devices) and deduce that only 80% of the geminate pairs are fully separated, at short circuit. Finally, charge extraction is nearly 100% efficient for this device, under the same conditions.

It is, thus, clear that the opportunities for improvement lie in four main areas. First, reflection must be reduced. Second, thicker nanostructures will allow for more light to be absorbed. Third, *a*-Si:H should be replaced with a nonabsorbing electron acceptor such as titania or an active absorber that contributes to the photocurrent. Finally, exciton harvesting at the interfaces must still be improved. Despite photocurrent enhancements due to nanostructuring, it is clear that more than half of the excitons within the pores are still unable to diffuse to the interface before their natural decay within the polymer. In the best nanostructured devices, pore sizes are still 30–40 nm wide, much larger than the optimal value of twice the exciton diffusion length in P3HT ($L_{diffusion}$=3 nm). Possible solutions are to make the pore

sizes smaller and/or to increase the effective exciton harvesting distances, perhaps by employing energy transfer.[15] Based on the P3HT absorption curves, a maximum J_{SC} of approximately 16 mA/cm^2 (including reflection losses) can be collected at the electrodes, if all collection steps are perfectly efficient.[39]

CONCLUSIONS

In conclusion, we have shown that efficient energy transfer can occur between polymers and *a*-Si:H, but that hole transfer from *a*-Si:H to the polymer can be inhibited by hole trapping deep in the *a*-Si:H valence bandtail. The deleterious hole transfer, unless overcome, renders *a*-Si:H unsuitable for use in polymer-based hybrid solar cells. We have also shown that nanostructured inorganic/polymer hybrid solar cells represent a promising route for fabricating organic-based solar cells with increased efficiencies. We have critically analyzed the various limitations in our best device and have proposed possible solutions. In light of these findings, we emphasize the importance of evaluating the valence band (HOMO)–valence band (HOMO) offsets and hole transfer, before designing novel semiconductor combinations for solar cell applications. Small exciton diffusion lengths in polymers pose a considerable challenge for the creation of adequately closely spaced nanostructures that lead to the efficient harvesting of excitons. Larger effective diffusion lengths in polymers would alleviate the stringent requirements that nanostructures must presently meet for efficient exciton harvesting, while making it easier to use a variety of inorganic scaffold materials for which advanced nanoscale lithography, RIE, or other techniques are not available. Finally, in order to make nanostructured hybrid solar cells efficient and commercially viable, further research, going beyond the scope of this work, is needed to explore and understand optimum nanostructure dimensions, exciton and charge dynamics at the nanoscale, and low-cost, high-throughput nanostructure fabrication techniques.

ACKNOWLEDGMENTS

The authors acknowledge the Center on Polymer Interfaces and Macromolecular Assemblies (CPIMA), the U.S. Department of Energy (DOE), and Global Climate and Energy Project (GCEP) at Stanford University for funding this project at various stages. NREL work was supported by the U.S. DOE under Contract No. DE-AC36-99GO10337.

[1]P. Peumans, A. Yakimov, and S. R. Forrest, J. Appl. Phys. **93**, 3693 (2003).
[2]J. G. Xue, S. Uchida, B. P. Rand, and S. R. Forrest, Appl. Phys. Lett. **85**, 5757 (2004).
[3]M. M. Koetse, J. Sweelssen, K. T. Hoekerd, H. F. M. Schoo, S. C. Veenstra, J. M. Kroon, X. Yang, and J. Loos, Appl. Phys. Lett. **88**, 083504 (2006).
[4]J. J. M. Halls, C. A. Walsh, N. C. Greenham, and E. A. Marseglia, Nature (London) **376**, 498 (1995).
[5]W. U. Huynh, J. J. Dittmer, and A. P. Alivisatos, Science **295**, 2425 (2002).
[6]B. Q. Sun, E. Marx, and N. C. Greenham, Nano Lett. **3**, 961 (2003).
[7]W. J. E. Beek, M. M. Wienk, M. Kemerink, X. Yang, and R. A. J. Janssen, J. Phys. Chem. B **109**, 9505 (2005).
[8]P. Ravirajan, S. A. Haque, J. R. Durrant, D. D. C. Bradley, and J. Nelson, Adv. Funct. Mater. **15**, 609 (2005).
[9]G. Li, V. Shrotriya, J. S. Huang, Y. Yao, T. Moriarty, K. Emery, and Y. Yang, Nat. Mater. **4**, 864 (2005).
[10]W. L. Ma, C. Y. Yang, X. Gong, K. Lee, and A. J. Heeger, Adv. Funct. Mater. **15**, 1617 (2005).
[11]V. D. Mihailetchi, H. X. Xie, B. de Boer, L. J. A. Koster, and P. W. M. Blom, Adv. Funct. Mater. **16**, 699 (2006).
[12]G. Yu, J. Gao, J. C. Hummelen, F. Wudl, and A. J. Heeger, Science **270**, 1789 (1995).
[13]K. M. Coakley, B. S. Srinivasan, J. M. Ziebarth, C. Goh, Y. X. Liu, and M. D. McGehee, Adv. Funct. Mater. **15**, 1927 (2005).
[14]Y. X. Liu, M. A. Summers, C. Edder, J. M. J. Frechet, and M. D. McGehee, Adv. Mater. (Weinheim, Ger.) **17**, 2960 (2005).
[15]S. R. Scully, P. B. Armstrong, C. Edder, J. M. J. Frechet, and M. D. McGehee, Adv. Mater. (Weinheim, Ger.) **19**, 2961.
[16]C. Goh, S. R. Scully, and M. D. McGehee, J. Appl. Phys. **101**, 114503 (2007).
[17]H. Fritzsche, Annu. Rev. Mater. Res. **31**, 47 (2001).
[18]K. M. Coakley and M. D. McGehee, Appl. Phys. Lett. **83**, 3380 (2003).
[19]D. C. Olson, J. Piris, R. T. Collins, S. E. Shaheen, and D. S. Ginley, Thin Solid Films **496**, 26 (2006).
[20]P. Ravirajan, A. M. Peiro, M. K. Nazeeruddin, M. Graetzel, D. D. C. Bradley, J. R. Durrant, and J. Nelson, J. Phys. Chem. B **110**, 7635 (2006).
[21]Q. Wang, E. Iwaniczko, Y. Xu, W. Gao, B. P. Nelson, A. H. Mahan, R. S. Crandall, and H. M. Branz, MRS Symposia Proceedings No. 609 (Materials Research Society, Pittsburgh, 2000), pp. A431–A436.
[22]V. Gowrishankar, S. R. Scully, M. D. McGehee, Q. Wang, and H. M. Branz, Appl. Phys. Lett. **89**, 252102 (2006).
[23]Y. X. Liu, S. R. Scully, M. D. McGehee, J. S. Liu, C. K. Luscombe, J. M. J. Frechet, S. E. Shaheen, and D. S. Ginley, J. Phys. Chem. B **110**, 3257 (2006).
[24]V. Gowrishankar, N. Miller, M. D. McGehee, M. J. Misner, D. Y. Ryu, T. P. Russell, E. Drockenmuller, and C. J. Hawker, Thin Solid Films **513**, 289 (2006).
[25]K. M. Coakley, Y. X. Liu, M. D. McGehee, K. L. Frindell, and G. D. Stucky, Adv. Funct. Mater. **13**, 301 (2003).
[26]R. A. Street, *Hydrogenated Amorphous Silicon*, edited by J. I. Pankove (Academic, London, 1984), Vol. B, pp. 203–207.
[27]T. Forster, Discuss. Faraday Soc. **27**, 7 (1959).
[28]A. J. Breeze, Z. Schlesinger, S. A. Carter, and P. J. Brock, Phys. Rev. B **64**, 125205 (2001).
[29]R. A. Street, *Hydrogenated Amorphous Silicon*, 1st ed. (Cambridge University Press, Cambridge, 1991), pp. 62–94 and 237–242.
[30]M. Stavola, D. L. Dexter, and R. S. Knox, Phys. Rev. B **31**, 2277 (1985).
[31]A. P. Alivisatos, M. F. Arndt, S. Efrima, D. H. Waldeck, and C. B. Harris, J. Chem. Phys. **86**, 6540 (1987).
[32]S. R. Scully and M. D. McGehee, J. Appl. Phys. **100**, 34907 (2006).
[33]E. A. Schiff, Sol. Energy Mater. Sol. Cells **78**, 567 (2003).
[34]V. D. Mihailetchi, L. J. A. Koster, J. C. Hummelen, and P. W. M. Blom, Phys. Rev. Lett. **93**, 216601 (2004).
[35]P. Peumans and S. R. Forrest, Chem. Phys. Lett. **398**, 27 (2004).
[36]V. D. Mihailetchi, J. Wildeman, and P. W. M. Blom, Phys. Rev. Lett. **94**, 126602 (2005).
[37]L. J. A. Koster, V. D. Mihailetchi, H. Xie, and P. W. M. Blom, Appl. Phys. Lett. **87**, 203502 (2005).
[38]P. Schilinsky, C. Waldauf, and C. J. Brabec, Appl. Phys. Lett. **81**, 3885 (2002).
[39]K. M. Coakley and M. D. McGehee, Chem. Mater. **16**, 4533 (2004).